

This work is on a Creative Commons Attribution-NonCommercial-NoDerivatives 4.0 International (CC BY-NC-ND 4.0) license, <https://creativecommons.org/licenses/by-nc-nd/4.0/>. Access to this work was provided by the University of Maryland, Baltimore County (UMBC) ScholarWorks@UMBC digital repository on the Maryland Shared Open Access (MD-SOAR) platform.

Please provide feedback

Please support the ScholarWorks@UMBC repository by emailing scholarworks-group@umbc.edu and telling us what having access to this work means to you and why it's important to you. Thank you.

Supplemental information

HIV-1 matrix-tRNA complex structure

reveals basis for host control of Gag localization

Charles Bou-Nader, Frauke Muecksch, Janae B. Brown, Jackson M. Gordon, Ashley York, Chen Peng, Rodolfo Ghirlando, Michael F. Summers, Paul D. Bieniasz, and Jinwei Zhang

Supplemental Figures and Tables

HIV-1 Matrix-tRNA complex structure reveals basis for host control of Gag localization

Charles Bou-Nader, Frauke Muecksch, Janae B. Brown, Jackson M. Gordon, Ashley York, Chen Peng, Rodolfo Ghirlando, Michael F. Summers, Paul D. Bieniasz, and Jinwei Zhang

Supplemental Tables S1-S3.

Supplemental Figures S1-S7.

Co-crystal structure of HIV-1 MA in complex with human tRNA ^{Lys3} PDB: 7MRL	
Data collection	
Space group	I 2 2 2
Cell dimensions	
<i>a</i> , <i>b</i> , <i>c</i> (Å)	96.717, 108.846, 146.021
α , β , γ (°)	90, 90, 90
Resolution (Å)	45.11- 3.15 (3.263-3.15)
<i>R</i> _{merge}	0.2103 (3.357)
<i>I</i> / σ <i>I</i>	8.7 (1.23)
CC _{1/2}	0.998 (0.576)
CC*	0.999 (0.855)
Completeness (%)	99.74 (99.55)
Redundancy	18.6 (17.5)
Refinement	
No. reflections	253812 (23158)
<i>R</i> _{work} / <i>R</i> _{free}	0.1885 (0.3611) / 0.2252 (0.3756)
No. atoms	
Macromolecules	3243
Mg ions	1
Water	5
<i>B</i> -factors	
Macromolecules	118.31
Mg ions	71.27
Water	88.14
R.m.s. deviations	
Bond lengths (Å)	0.003
Bond angles (°)	0.52

Table S1. Summary of data collection and refinement statistics for the co-crystal structure of HIV-1 MA bound to human tRNA^{Lys3}, Related to Figure 2.

tRNA in cell	Titrant (MA)	K_d (μ M)	Log(K_a)	ΔH (kcal.mol ⁻¹)	- ΔS (kcal.mol ⁻¹)
WT tRNA ^{Lys3}	WT	0.267 \pm 0.02	6.57 \pm 0.04	-4.65 \pm 0.8	-0.165 \pm 1
	K18A	0.32 \pm 0.14	6.51 \pm 0.19	-12.4 \pm 1.5	-7.8 \pm 1.7
	R20A	0.49 \pm 0.16	6.32 \pm 0.16	-10 \pm 1.8	-12 \pm 1.6
	R22A	25.6 \pm 5.9	4.62 \pm 0.2	N.D.	
	K26A	1.6 \pm 0.58	5.8 \pm 0.16	-9.2 \pm 2.4	-20 \pm 1.8
	K27A	49.8 \pm 6.8	4.31 \pm 0.07	N.D.	
	K30A	1.15 \pm 0.54	5.97 \pm 0.23	-11.05 \pm 0.2	-11 \pm 1.4
	K32A	N.D.			
	H33A	7.5 \pm 1.6	5.13 \pm 0.1	N.D.	
	W36F	44.4 \pm 10.2	4.36 \pm 0.14	N.D.	
	W36A	N.D.			
	E73A	0.22 \pm 0.04	6.67 \pm 0.08	-6.7 \pm 1.0	-3.97 \pm 1.1
	E74A	1.45 \pm 0.24	5.84 \pm 0.07	-6.15 \pm 2.1	-4.05 \pm 2.05
	R76A	4.5 \pm 2.1	5.37 \pm 0.21	-3.65 \pm 1	-0.18 \pm 1.2
	S77L	N.D.			
	S77A	1.13 \pm 0.5	5.98 \pm 0.18	-4.6 \pm 1.4	-0.88 \pm 0.8
tG19C	WT	90 \pm 30	4.06 \pm 0.15	N.D.	
tU20C		0.52 \pm 0.1	6.29 \pm 0.09	-6.5 \pm 2.7	-2 \pm 2
tU20A		1.23 \pm 0.18	5.91 \pm 0.06	-4.2 \pm 0.25	0.73 \pm 1.4
tU20G		1.12 \pm 0.5	5.98 \pm 0.18	-4.6 \pm 1.4	1.08 \pm 0.5
tU55C		33.9 \pm 12.7	4.5 \pm 0.17	N.D.	
tC56G		40.5 \pm 4.8	4.39 \pm 0.05	N.D.	
tG19C:tC56G		13.4 \pm 4.4	4.89 \pm 0.16	-10 \pm 3	-3 \pm 2
tA7U:U66A		0.61 \pm 0.16	6.22 \pm 0.1	-7.7 \pm 0.15	1.1 \pm 0.2
tU8C		19.5 \pm 7.2	4.73 \pm 0.16	-16.5 \pm 5	-13 \pm 5
tA9U		3.71 \pm 0.5	5.43 \pm 0.05	-13.5 \pm 6	-9.5 \pm 6.2
tG15C		10.2 \pm 0.8	4.99 \pm 0.03	-13.75 \pm 3	-10.5 \pm 3
tC48G		0.69 \pm 0.01	6.16 \pm 0.01	-8.2 \pm 2.2	-3.85 \pm 2.2
tG15C:tC48G		2.29 \pm 0.09	5.63 \pm 0.02	-19.5 \pm 1.3	-15.5 \pm 1.3
ASL GAAA		0.89 \pm 0.5	6.09 \pm 0.22	-11.3 \pm 1.2	-1.4 \pm 1.5
t Δ C17/ins tU20a		0.49 \pm 0.08	6.31 \pm 0.07	-2.1 \pm 0.01	-6.5 \pm 0.08
tC17U		0.43 \pm 0.1	6.34 \pm 0.1	-2.27 \pm 0.05	-6.34 \pm 0.1
tC17U/tU20G		0.92 \pm 0.01	6.03 \pm 0.001	-1.77 \pm 0.4	-6.4 \pm 0.4
tC17U/ins tU20a		0.38 \pm 0.05	6.417 \pm 0.01	-1.64 \pm 0.5	-7.12 \pm 0.8
tA57G		0.98 \pm 0.4	6.03 \pm 0.18	-0.89 \pm 0.3	-7.33 \pm 0.51
tC13G/t Δ C17/ins tU20a/tG22A		N.D.			
tRNA ^{Phe}		1.8 \pm 0.9	5.81 \pm 0.28	-2.4 \pm 0.1	-5.5 \pm 0.5
tRNA ^{Gly}		1.84 \pm 0.3	5.74 \pm 0.06	-4.12 \pm 0.13	-3.7 \pm 0.09
tRNA ^{Thr} Site 1		0.5	6.3	N.D.	
tRNA ^{Thr} Site 2		7.2	5.1	N.D.	
tRNA ^{Thr} G19C		2.7 \pm 0.5	5.6 \pm 0.09	-10.5 \pm 5	-2.9 \pm 5
tRNA ^{Leu} Site 1		1.0	6.0	N.D.	
tRNA ^{Leu} Site 2		5.8	5.2	N.D.	
tRNA ^{Ser} Site 1		1.5	5.8	N.D.	
tRNA ^{Ser} Site 2		15	4.8	N.D.	

Table S2. Summary of ITC parameters for tRNA^{Lys3} binding to HIV-1 MA, Related to Figures 1 and 3.

K_d values are mean \pm s.d. (n=3 for WT tRNA^{Lys3} titrated with WT, K18A, R20A, R22A, K27A, K30A, K32A, H33A, W36A, E73A, E74A, R76A, S77L, S77A MA variants and for titration of WT MA with tU8C, tU20C, tU20G, tU55C, tG19C:C56G, tA7U:U66A, ASL-GAAA tRNA^{Lys3} variants and tRNA^{Thr}, tRNA^{Gly}, tRNA^{Phe}, tRNA^{Ser}, tRNA^{Leu}; n=2 for tRNA^{Lys3} titrated with K26A, W36F MA variants and for titration of WT MA with tA9U, tG15C, tG19C, tU20A, tC56G, tC48G, tG15C:C48G, t Δ C17/ins_tU20a, tC17U, tC17U/tU20G, tC17U/ins_tU20a, tA57G, tC13G/t Δ C17/ins_tU20a/tG22A, tRNA^{Thr} G19C). “ins_tU20a” denotes the insertion of a U residue after tU20. This insertion is frequently observed in some tRNAs and referred to as “U20a” by conventional tRNA numbering. N.D.: not determined due to weak binding. For biphasic isotherms (tRNA^{Leu}, tRNA^{Ser}, tRNA^{Thr}), triplicate titration data were globally fit to a two-site non-symmetric model yielding two dissociation constants.

tRNA	MA	tRNA:MA Ratio	[tRNA] (μ M)	[MA] (μ M)	Sedimentation coefficient (S) ^{a,b}	Estimated molar mass (kDa) ^c
--	WT	--	--	32	1.63	11.9
--	K32A	--	--	36	1.69	14.9
tRNA ^{Lys3}	--	--	3.3	--	4.48	25.5
tRNA ^{Lys3}	WT	1:1	3.3	3.3	4.73	37.5
tRNA ^{Lys3}	WT	1:4	3.3	13.3	4.82	40.2
tRNA ^{Lys3}	WT	1:3 ^d	35	105	4.77	42.3
tRNA ^{Lys3}	WT	1:5 ^d	35	175	4.83	44.4
tRNA ^{Lys3}	K32A	1:1	3.3	3.6	4.47	27.2
tRNA ^{Lys3}	K32A	1:4	3.3	14.8	4.48	25.4
tRNA ^{Leu}	--	--	3.2	--	4.87	32.4
tRNA ^{Leu}	WT	1:1	2.8	3.2	5.05	40.4
tRNA ^{Leu}	WT	1:2	2.8	6.6	5.19	45.1
tRNA ^{Leu}	WT	1:4	2.8	13.3	5.23	49.8
tRNA ^{Leu}	K32A	1:1	2.5	2.7	4.87	30.7
tRNA ^{Leu}	K32A	1:2	2.5	5.0	4.86	31.5
tRNA ^{Leu}	K32A	1:4	2.5	11.0	4.87	32.3
tRNA ^{Ser}	--	--	2.5	--	4.86	34.4
tRNA ^{Ser}	WT	1:1	2.5	3.2	5.04	46.8
tRNA ^{Ser}	WT	1:2	2.5	6.5	5.13	47.0
tRNA ^{Ser}	WT	1:4	2.5	13.3	5.25	51.4
tRNA ^{Thr}	--	--	2.5	--	4.60	30.7
tRNA ^{Thr}	WT	1:1	2.5	3.2	4.75	39.9
tRNA ^{Thr}	WT	1:2	2.5	6.3	4.87	41.8
tRNA ^{Thr}	WT	1:4	2.5	12.7	4.97	52.5
tRNA ^{Thr}	K32A	1:1	2.5	2.7	4.65	30.6
tRNA ^{Thr}	K32A	1:2	2.5	5.2	4.63	31.0
tRNA ^{Thr}	K32A	1:4	2.5	11.0	4.62	32.0

Table S3. Summary of AUC sedimentation coefficients and estimated molar masses, Related to Figures 1 and 3.

^aExperimental sedimentation coefficients at 25°C. For the tRNA:MA complexes, the faster sedimentation coefficient of the free or complexed tRNA is shown, together with the estimated molar mass. The sedimentation coefficient for the free protein is not reported.

^bThe error on the experimental Sedimentation coefficient is ± 0.02 S.

^cMasses are based on partial specific volumes of 0.7412 cm³/g for the protein, 0.55 cm³/g for tRNA, and 0.6123 cm³/g for the 1:1 tRNA:MA complex.

^dHigh-concentration samples were prepared by mixing SEC-purified 1:1 complex with excess MA.

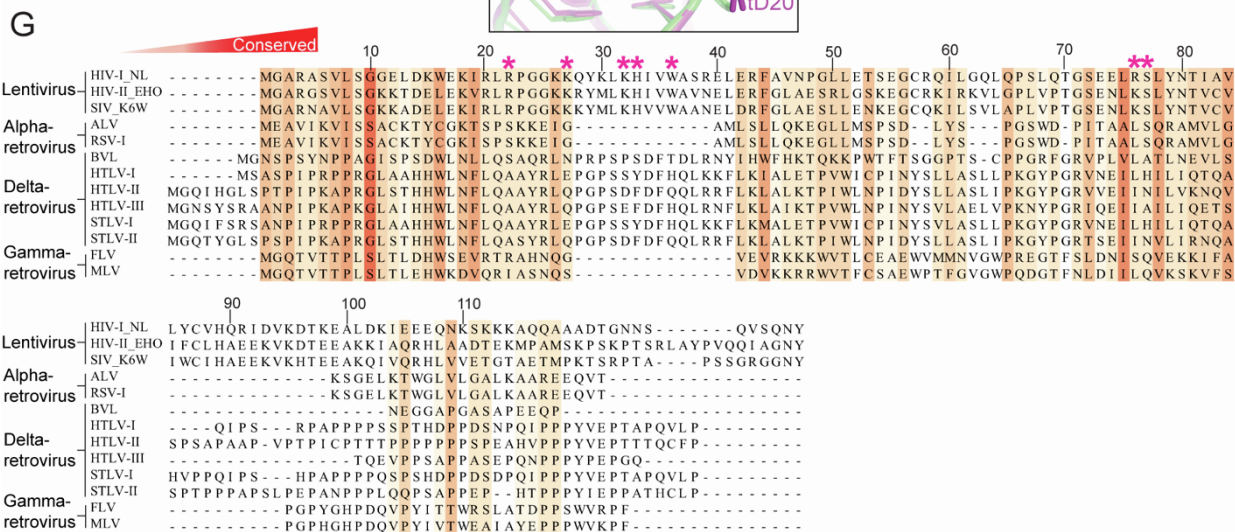
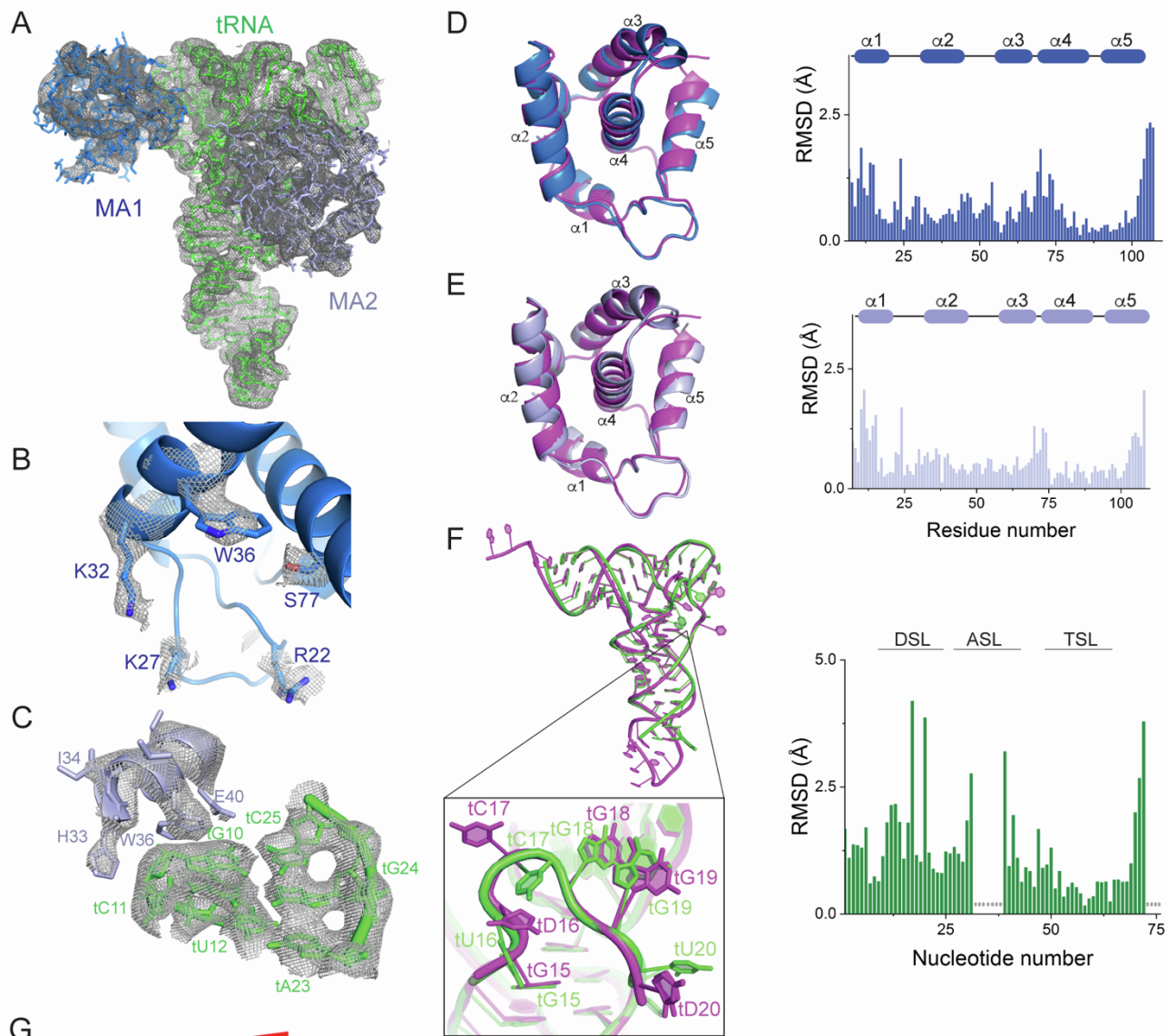


Figure S1. Representative electron density maps, sequence alignment, and structural comparisons with isolated MA and tRNA structures, Related to Figures 2 and 3.

(A) Composite simulated anneal-omit 2Fo-Fc density calculated using the final model and superimposed with the final refined model contoured at 1σ .

(B) Portion of the map showing the MA interface at the tRNA elbow region. Residues in contact with tRNA are shown in sticks. tRNA is omitted for clarity.

(C) Portion of the map showing MA interface with the tRNA inner corner. tRNA^{Lys3} residues are numbered according to standard convention (with a 't' prefix) and in parentheses are the numbers used in the deposited PDB coordinates. The numbering difference is due to the engineering of the tRNA anticodon stem loop (ASL) for crystallization.

(D) Left: superposition of MA bound to the tRNA elbow region (blue) with the trimeric MA crystal structure (PDB:1HIW, magenta) (Hill et al., 1996). Right: distribution of RMSDs between corresponding residues with an overall RMSD of 0.6 Å over 89 residues.

(E) Left: superposition of MA bound to the tRNA inner corner (light blue) with the trimeric MA crystal structure (magenta). Right: distribution of RMSDs between corresponding residues with an average RMSD of 0.5 Å over 89 residues.

(F) Left: superposition of the tRNA molecule bound to MA (green) with an isolated tRNA^{Lys3} structure (PDB:1FIR, magenta) (Benas et al., 2000). Right: distribution of RMSDs between corresponding residues, with an overall RMSD of 2.1 Å over 64 residues. The engineered portion of the tRNA ASL for crystallization (asterisks) was excluded from this analysis.

(G) Sequence alignment of representative retroviruses. *Residues interacting with tRNA.

(H) Structural comparison of HIV-1 MA (left; PDB 1HIW) (Hill et al., 1996), HIV-2 MA (middle; PDB 2K4E) (Saad et al., 2008), and SIV MA (right; PDB 1ED1) (Rao et al., 1995). tRNA-binding residues shown as magenta sticks.

(I) Electrophoretic mobility shift assay (EMSA) showing that MA binds stoichiometrically to tRNA^{Lys3}.

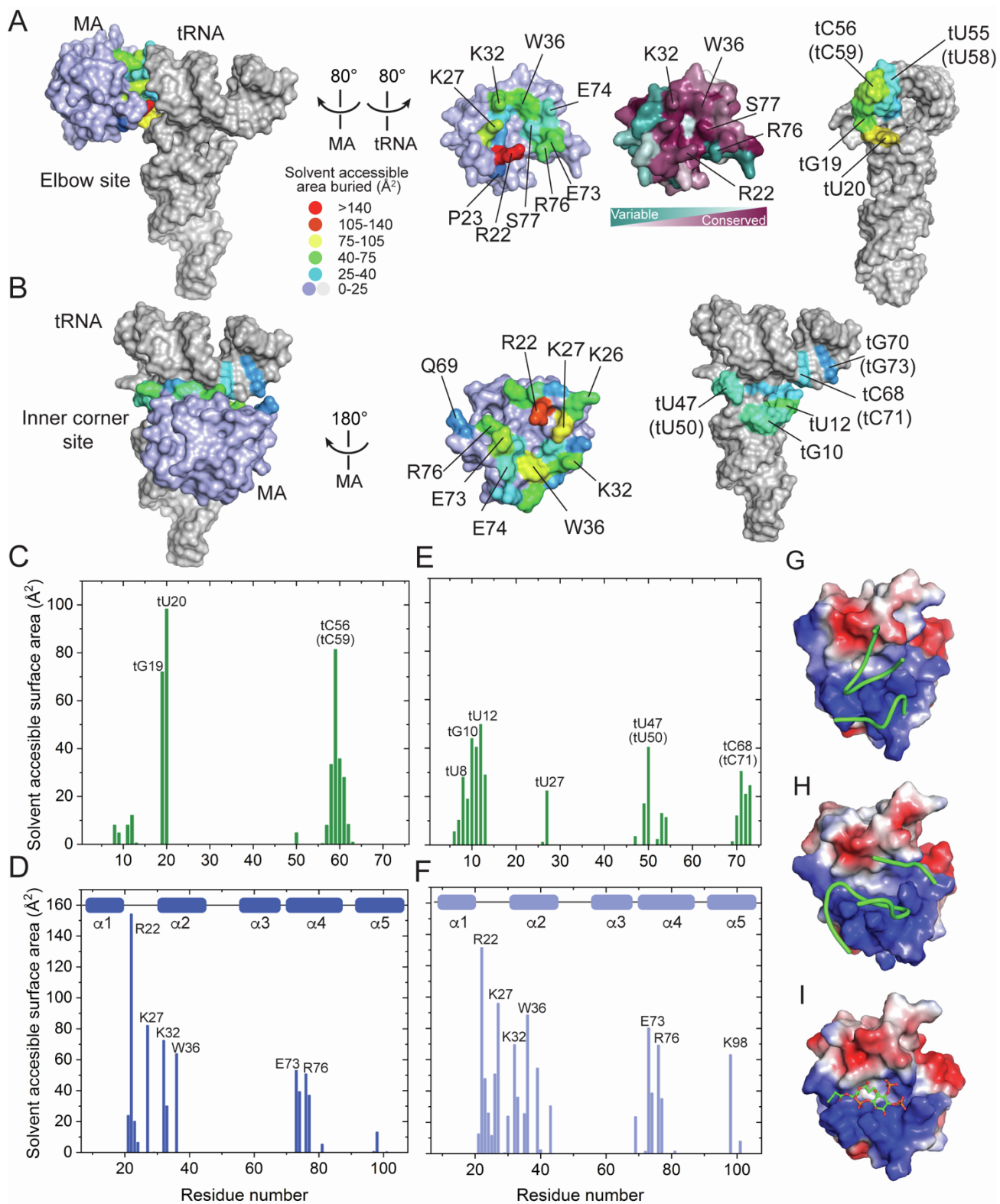


Figure S2. Intermolecular interface of the tRNA^{Lys3}-MA complex, Related to Figure 2.

(A) Open-book view of the tRNA elbow-MA interface. Left: solvent-accessible surface colored according to area buried from light blue or white (no burial) to red ($>140 \text{ \AA}^2$ per residue). Right: Rotated views of the binding interfaces. tRNA^{Lys3} residues are numbered according to standard convention (with a 't' prefix). Numbers in parentheses are those used in the deposited PDB coordinates. Conservation of MA residues was calculated using ConSurf (Landau et al., 2005).

(B) Open-book view of the tRNA inner corner-MA interface. Colored as in (A).

(C, D) Plots of solvent-accessible surface area buried per residue (\AA^2) on tRNA^{Lys3} (C) and MA (D) at the elbow site.

(E, F) Plots of solvent-accessible surface area buried per residue (\AA^2) on tRNA^{Lys3} (E) and MA (F) at the inner corner site.

(G-I) Electrostatic surface of MA binding interfaces with the tRNA^{Lys3} inner corner (G), elbow (H), and di-C4-phosphatidylinositol-(4,5)-biphosphate (I; PDB: 2H3Z) (Saad et al., 2006). The RNA backbone is shown in green. Positive charges are shown in blue and negative charges in red.

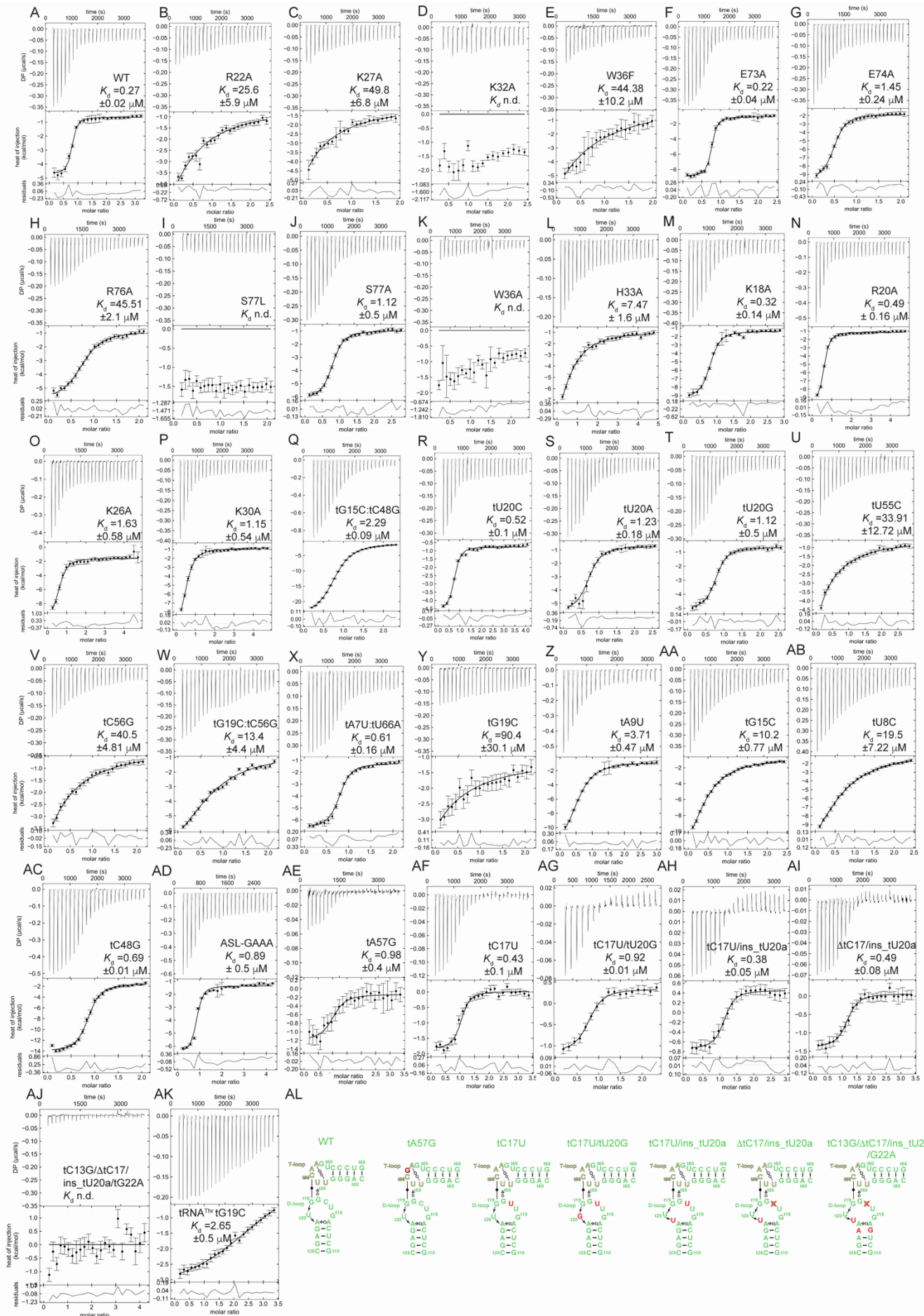


Figure S3. Representative ITC isotherms for tRNA^{Lys3} binding to HIV-1 MA, Related to Figure 3.

(A-P) Representative ITC isotherms for tRNA^{Lys3} binding to (A) WT, (B) R22A, (C) K27A, (D) K32A, (E) W36F, (F) E73A, (G) E74A, (H) R76A, (I) S77L, (J) S77A, (K) W36A, (L) H33A, (M) K18A, (N) R20A, (O) K26A, (P) K30A MA variants.

(Q-AK) Representative ITC isotherms for WT MA binding to (Q) tG15C:C48G, (R) tU20C, (S) tU20A, (T) tU20G, (U) tU55G, (V) tC56G, (W) tG19C:tC56G, (X) tA7U:tU66A, (Y) tG19C, (Z) tA9U, (AA) tG15C, (AB) tU8C, (AC) tC48G, (AD) ASL-GAAA (crystallization construct), (AE) tA57G, (AF) tC17U, (AG) tC17U/tU20G (harboring the D-loop of tRNA^{Phe}), (AH) tC17U/ins_tU20a (harboring the D-loop of tRNA^{Thr}), (AI) ΔtC17/ins_tU20a, (AJ) tC13G/ΔtC17/ins_tU20a/tG22A (harboring the D-loop of tRNA^{Ser}) tRNA^{Lys3} variants and (AK) tRNA^{Thr} tG19C. “ins_tU20a” denotes the insertion of a U residue after tU20. This insertion is frequently observed in some tRNAs and referred to as “U20a” by conventional tRNA numbering. The constructs names and the K_d values (mean \pm s.d., n=3 for A, B, C, D, F, G, H, I, J, K, L, M, N, P, R, T, U, W, X, AB, AD; n=2 for E, O, Q, S, V, Y, Z, AA, AC, AE, AF, AG, AH, AI, AJ, AK) are indicated in the top panels of the ITC isotherms. See also Fig. 3 and Table S2.

(AL) Secondary structures of the elbow regions of WT and chimeric tRNA^{Lys3} variants that harbor D-loop sequences from other tRNAs. See also Figure 3D.

The error bars indicate uncertainties in individual injection heats estimated by NITPIC (STAR Methods).

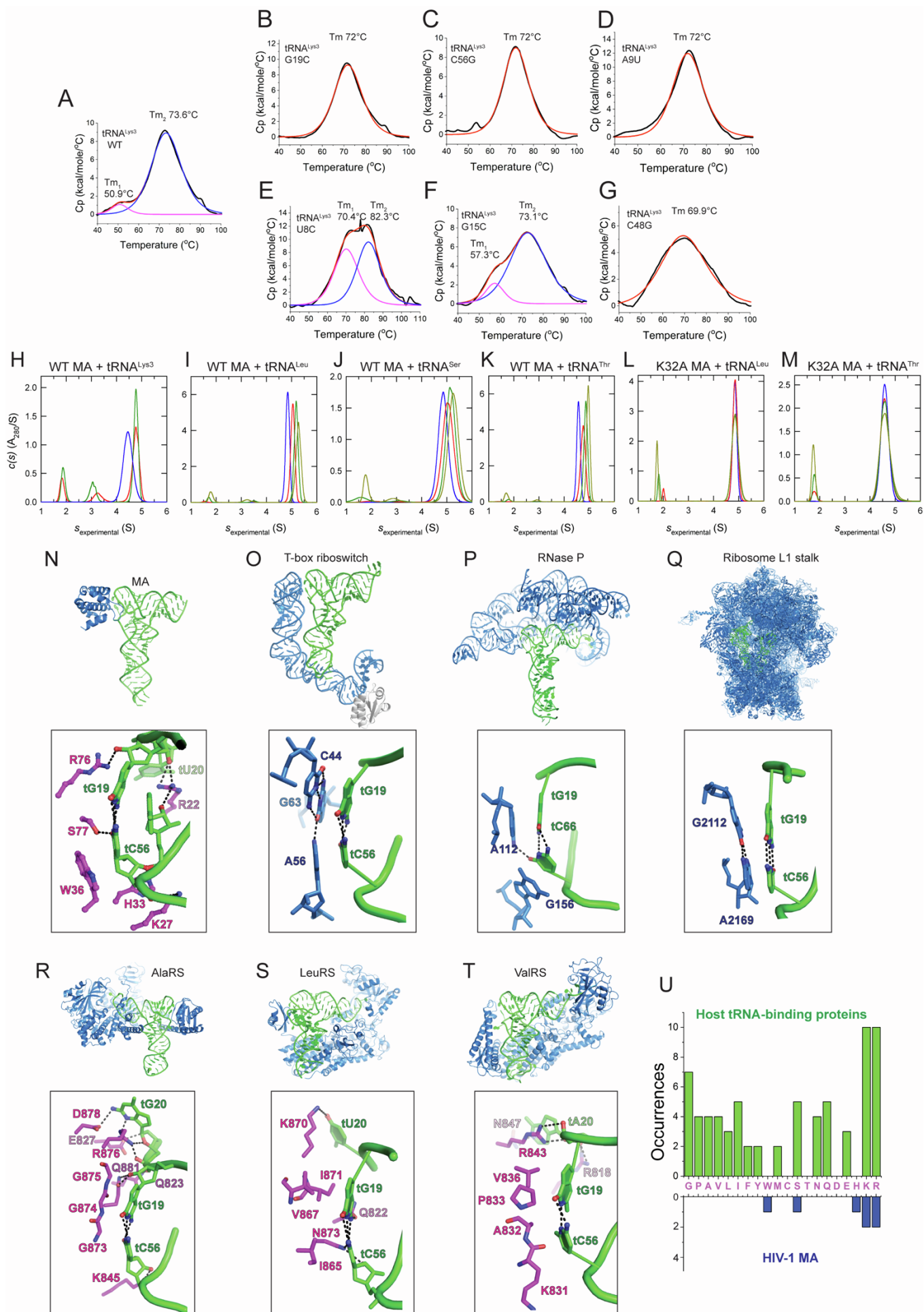


Figure S4. DSC analysis of tRNA^{Lys3} variants, AUC analysis of tRNA-MA complexes, and structural comparison of tRNA elbow recognition by MA with host RNAs and proteins, Related to Figures 2 and 3.

(A) Differential scanning calorimetry (DSC) analysis of the unfolding profile of WT tRNA^{Lys3}. T_m values (melting temperatures) are indicated.

(B) DSC unfolding profile of tRNA^{Lys3} tG19C.

(C) DSC unfolding profile of tRNA^{Lys3} tC56G.

(D) DSC unfolding profile of tRNA^{Lys3} tA9U.

(E) DSC unfolding profile of tRNA^{Lys3} tU8C.

(F) DSC unfolding profile of tRNA^{Lys3} tG15C.

(G) DSC unfolding profile of tRNA^{Lys3} tC48G.

(H) Analytical ultracentrifugation (AUC) analysis of WT MA binding to tRNA^{Lys3} at elevated concentrations, showing data for free tRNA (blue), and tRNA with 3 (red) and 5 (green) molar equivalents of MA (Table S3)

(I) AUC analysis of WT MA binding to tRNA^{Leu}, showing data for free tRNA (blue), and tRNA with 1 (red), 2 (green), and 4 (yellow) molar equivalents of MA (Table S3)

(J) AUC analysis of WT MA binding to tRNA^{Ser}, colored as in (I)

(K) AUC analysis of WT MA binding to tRNA^{Thr}, colored as in (I)

(L) AUC analysis of K32A MA binding to tRNA^{Leu}, colored as in (I)

(M) AUC analysis of K32A MA binding to tRNA^{Ser}, colored as in (I)

(N) Recognition of tRNA elbow by HIV-1 MA (this work).

(O) *Bacillus subtilis* glyQS T-box riboswitch-tRNA complex (PDB 4LCK) (Zhang and Ferré-D'Amaré, 2013).

(P) *Thermotoga maritima* Ribonuclease P-pre-tRNA complex (PDB 3Q1Q) (Reiter et al., 2010).

(Q) *Thermus thermophilus* 70S ribosome (PDB 4V4I) (Korostelev et al., 2006).

(R) *Archaeoglobus fulgidus* alanyl-tRNA synthetase, AlaRS (PDB 3WQZ) (Naganuma et al., 2014).

(S) *Thermus thermophilus* leucyl-tRNA synthetase, LeuRS (PDB 2V0G) (Rock et al., 2007).

(T) *Thermus thermophilus* valyl-tRNA synthetase, ValRS (PDB 1GAX) (Fukai et al., 2000).

(U) Occurrences of amino acids used to recognize the elbow tertiary base pair by host proteins (upper graph) and HIV-1 MA (lower graph).

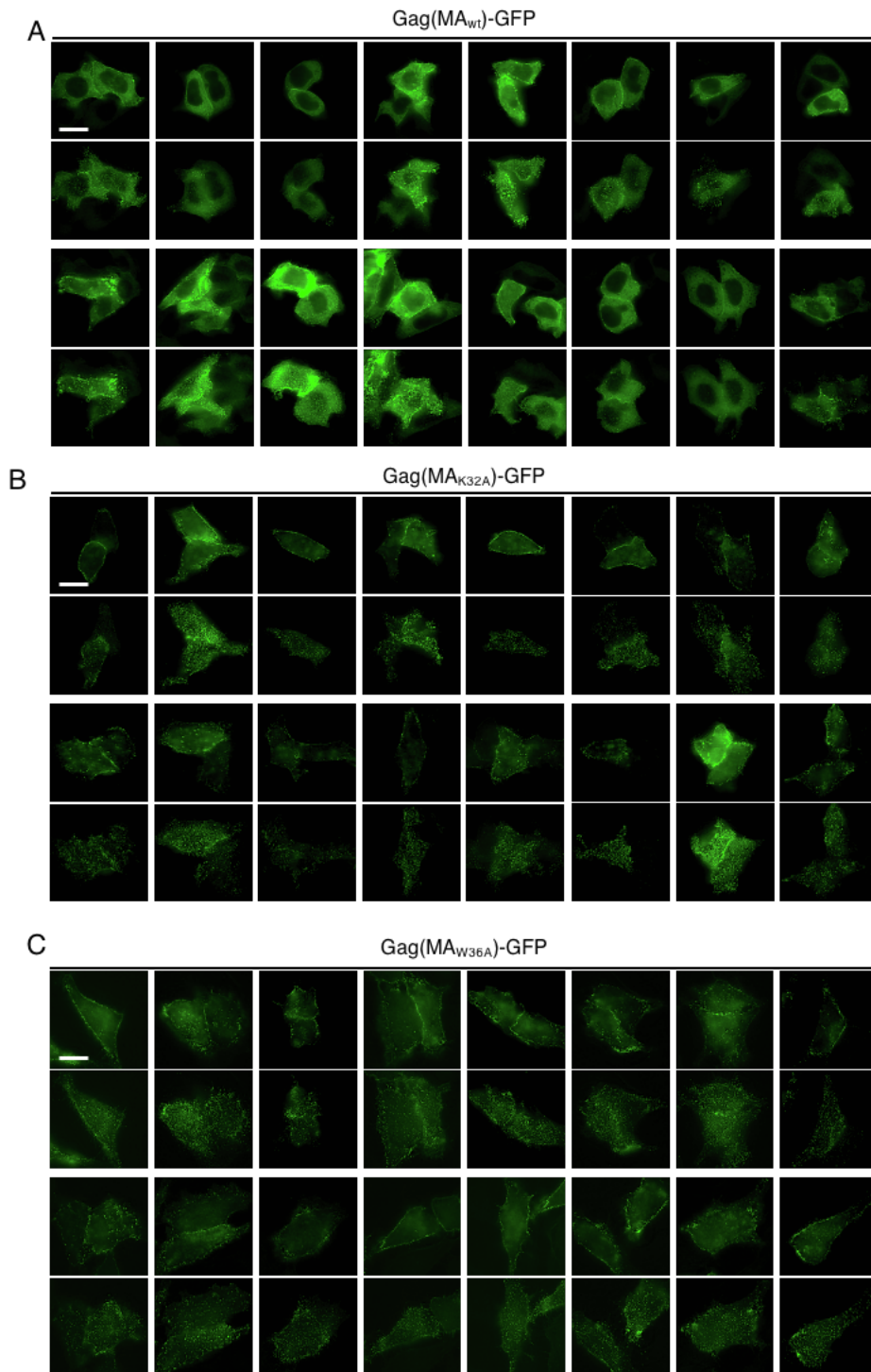


Figure S5. Effect of tRNA binding site mutation on Gag localization, Related to Figure 6.

(A - C) Representative widefield images of a central optical section (top panels) or ventral PM (bottom panels) of HeLa cells transfected with pCR3.1Gag(MA^{WT})-GFP (A), pCR3.1Gag(MA^{K32A})-GFP (B) or pCR3.1Gag(MA^{W36A})-GFP (C). Cells were fixed 12 hours after transfection. Scale bars indicate 20 μ m.

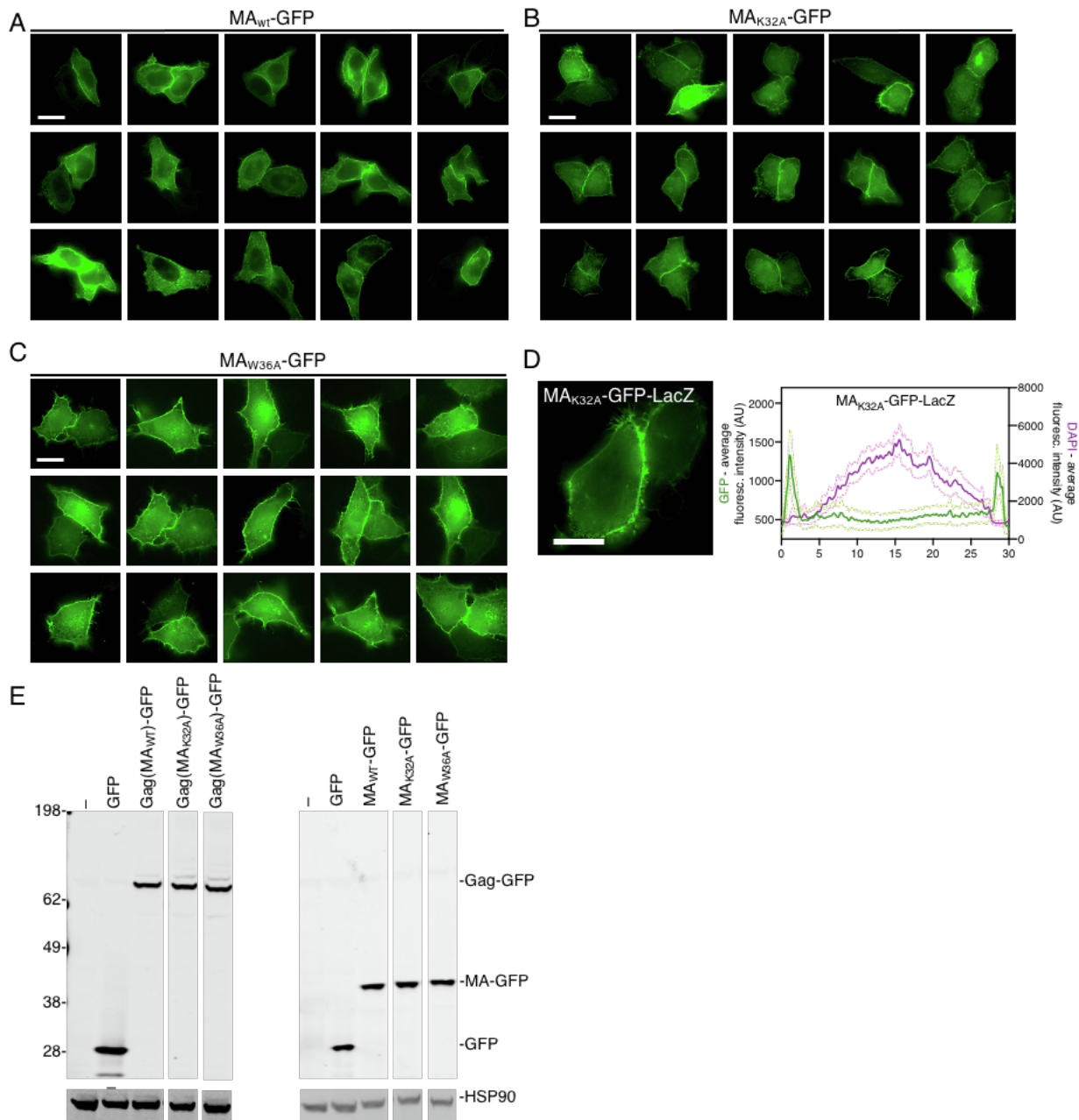


Figure S6. Effect of tRNA binding site mutation on MA-GFP localization, Related to Figure 6.

(A-D) Representative widefield images of a central optical section of HeLa cells transfected with pCR3.1MA^{WT}-GFP (A), pCR3.1MA(K32A)-GFP (B), pCR3.1MA(W36A)-GFP (C) or pCR3.1Gag(MA^{K32A})-GFP-LacZ (D). Cells were fixed 12 hours after transfection. Scale bars indicate 20 μ m. Images are displayed with adjusted brightness to facilitate visualization. Graph in (D) shows averaged line profiles of selected cells expressing MA^{K32A}-GFP-LacZ. Shown is the average fluorescence intensity (arbitrary units, AU) of GFP (green, left y-axis) or DAPI (magenta, right y-axis).

(E) Western blot (anti-GFP) analysis of Gag-GFP and MA-GFP fusion protein levels and integrity in transfected 293T cells.

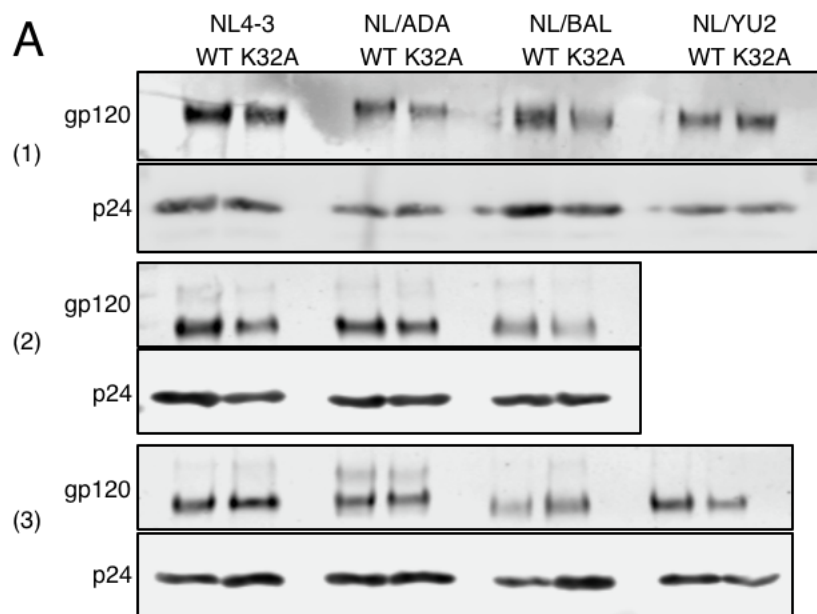
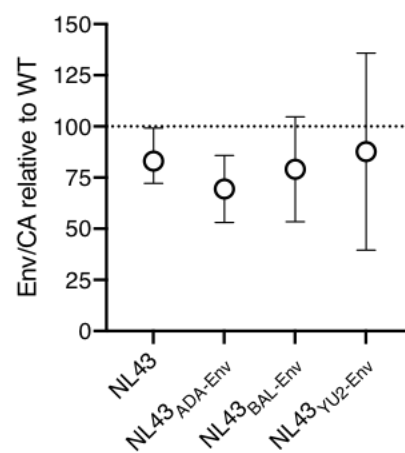
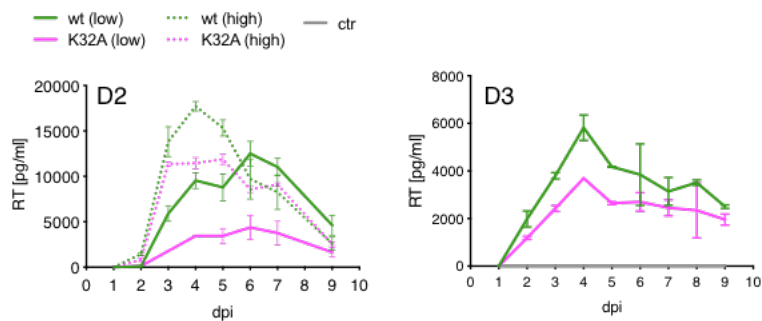
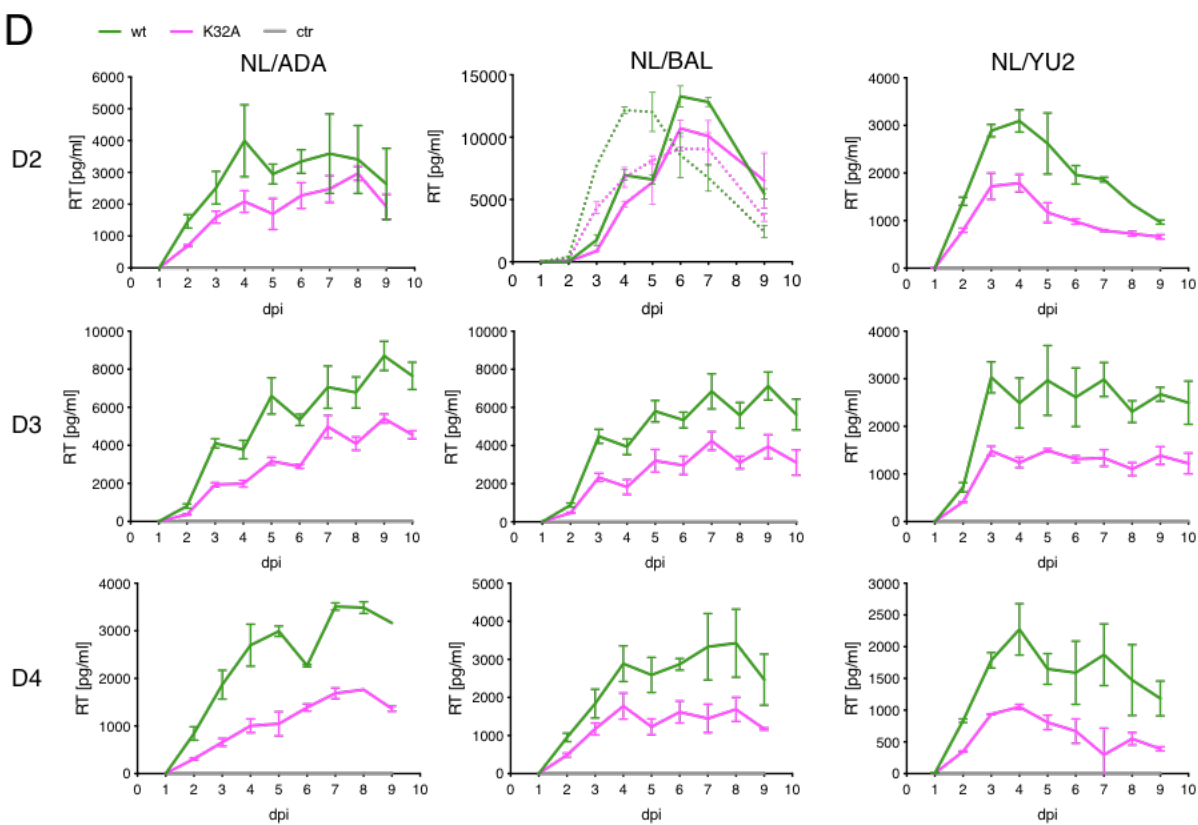
A**B****C****D**

Figure S7. Env-incorporation into MA-WT and MA-K32A HIV-1 particles and replication of WT and K32A mutant viruses in primary cells, Related to Figure 7.

(A) Additional examples of Env incorporation into virions from 293T cells infected with VSV-G-pseudotyped HIV-1NL4-3, HIV-1NL/ADA, HIV-1NL/BaL or HIV-1NL/Yu2 each encoding MA^{WT} or MA^{K32A}. Supernatants were harvested 48hpt, pelleted through a sucrose cushion and run on SDS-PAGE. Western blots probed with anti-Env and anti-p24 and respective secondary antibodies (A).

(B) Band-intensities of Env and p24 on western blots were quantified and Env-content was normalized to p24. Shown are relative Env/CA values in MA^{K32A} particles, normalized to those of MA^{WT} virus. Shown are mean values and range for n=4 experiments (n=3 for HIV-1NL/YU2).

(C) Reverse Transcriptase (RT) levels in supernatants of CD4⁺ T-cells from three donors (D2-D4) after infection with HIV-1NL4-3 MA^{WT} (green) or HIV-1NL4-3 MA^{K32A} (magenta) at 0.4 (dotted lines)/ 0.05 (continuous lines) MT4-LTR-GFP infectious units/cell. Supernatants harvested from uninfected cells are shown in grey.

(D) RT levels in supernatants of primary monocyte-derived macrophages from three donors (D2-D4) after infection with the R5-tropic HIV-1NL/ADA, HIV-1NL/BaL or HIV-1NL/Yu2 each encoding MA^{WT} (green) or MA^{K32A} (magenta), at 2.5 MT4-LTR-GFP infectious units/cell. Data are represented as mean \pm SEM.

References to Supplemental Figures

- Benas, P., Bec, G., Keith, G., Marquet, R., Ehresmann, C., Ehresmann, B., and Dumas, P. (2000). The crystal structure of HIV reverse-transcription primer tRNA(Lys,3) shows a canonical anticodon loop. *RNA* 6, 1347-1355.
- Fukai, S., Nureki, O., Sekine, S., Shimada, A., Tao, J., Vassylyev, D.G., and Yokoyama, S. (2000). Structural basis for double-sieve discrimination of L-valine from L-isoleucine and L-threonine by the complex of tRNA(Val) and valyl-tRNA synthetase. *Cell* 103, 793-803.
- Hill, C.P., Worthylake, D., Bancroft, D.P., Christensen, A.M., and Sundquist, W.I. (1996). Crystal structures of the trimeric human immunodeficiency virus type 1 matrix protein: implications for membrane association and assembly. *Proc Natl Acad Sci U S A* 93, 3099-3104.
- Korostelev, A., Trakhanov, S., Laurberg, M., and Noller, H.F. (2006). Crystal structure of a 70S ribosome-tRNA complex reveals functional interactions and rearrangements. *Cell* 126, 1065-1077.
- Landau, M., Mayrose, I., Rosenberg, Y., Glaser, F., Martz, E., Pupko, T., and Ben-Tal, N. (2005). ConSurf 2005: the projection of evolutionary conservation scores of residues on protein structures. *Nucleic Acids Res* 33, W299-302.
- Naganuma, M., Sekine, S., Chong, Y.E., Guo, M., Yang, X.L., Gamper, H., Hou, Y.M., Schimmel, P., and Yokoyama, S. (2014). The selective tRNA aminoacylation mechanism based on a single G*U pair. *Nature* 510, 507-511.
- Rao, Z., Belyaev, A.S., Fry, E., Roy, P., Jones, I.M., and Stuart, D.I. (1995). Crystal structure of SIV matrix antigen and implications for virus assembly. *Nature* 378, 743-747.
- Reiter, N.J., Osterman, A., Torres-Larios, A., Swinger, K.K., Pan, T., and Mondragon, A. (2010). Structure of a bacterial ribonuclease P holoenzyme in complex with tRNA. *Nature* 468, 784-789.
- Rock, F.L., Mao, W., Yaremchuk, A., Tukalo, M., Crepin, T., Zhou, H., Zhang, Y.K., Hernandez, V., Akama, T., Baker, S.J., *et al.* (2007). An antifungal agent inhibits an aminoacyl-tRNA synthetase by trapping tRNA in the editing site. *Science* 316, 1759-1761.
- Saad, J.S., Ablan, S.D., Ghanam, R.H., Kim, A., Andrews, K., Nagashima, K., Soheilian, F., Freed, E.O., and Summers, M.F. (2008). Structure of the myristylated human immunodeficiency virus type 2 matrix protein and the role of phosphatidylinositol-(4,5)-bisphosphate in membrane targeting. *J Mol Biol* 382, 434-447.
- Saad, J.S., Miller, J., Tai, J., Kim, A., Ghanam, R.H., and Summers, M.F. (2006). Structural basis for targeting HIV-1 Gag proteins to the plasma membrane for virus assembly. *Proc Natl Acad Sci U S A* 103, 11364-11369.
- Zhang, J., and Ferré-D'Amaré, A.R. (2013). Co-crystal structure of a T-box riboswitch stem I domain in complex with its cognate tRNA. *Nature* 500, 363-366.